800 *Inorg. Chem.* **2011**, *50*, 800–805
DOI: 10.1021/ic101961z

Inorganic Chemistry
Article

From Hollow Olive-Shaped $BiVO_4$ to n−p Core−Shell $BiVO_4$@Bi_2O_3 Microspheres: Controlled Synthesis and Enhanced Visible-Light-Responsive Photocatalytic Properties

Mei-Li Guan, De-Kun Ma,* Sheng-Wei Hu, Yan-Jun Chen, and Shao-Ming Huang*

Nanomaterials and Chemistry Key Laboratory, Wenzhou University, Wenzhou, Zhejiang 325027, People's Republic of China

Received July 8, 2010

In this study, hollow olive-shaped $BiVO_4$ and n−p core−shell $BiVO_4$@Bi_2O_3 microspheres were synthesized by a novel sodium bis(2-ethylhexyl)sulfosuccinate (AOT)-assisted mixed solvothermal route and a thermal solution of NaOH etching process under hydrothermal conditions for the first time, respectively. The as-obtained products were characterized by X-ray diffraction (XRD), scanning electron microscopy (SEM), transmission electron microscopy, Brunauer−Emmett−Teller surface area, and UV−vis diffuse-reflectance spectroscopy in detail. The influence of AOT and solvent ratios on the final products was studied. On the basis of SEM observations and XRD analyses of the samples synthesized at different reaction stages, the formation mechanism of hollow olive-shaped $BiVO_4$ microspheres was proposed. The photocatalytic activities of hollow olive-shaped $BiVO_4$ and core−shell $BiVO_4$@Bi_2O_3 microspheres were evaluated on the degradation of rhodamine B under visible-light irradiation (λ > 400 nm). The results indicated that core−shell $BiVO_4$@Bi_2O_3 exhibited much higher photocatalytic activities than pure olive-shaped $BiVO_4$. The mechanism of enhanced photocatalytic activity of core−shell $BiVO_4$@Bi_2O_3 microspheres was discussed on the basis of the calculated energy band positions as well. The present study provides a new strategy to enhancing the photocatalytic activity of visible-light-responsive Bi-based photocatalysts by p−n heterojunction.

Introduction

Materials with a hollow interior have attracted much attention compared to solid counterparts because they can be used to lower the density, enhance the specific surface area, modulate the refractive index, withstand cyclic changes in volume, and widely perform as drug delivery, catalysis, sensors, lightweight materials, and various new applications.[1] Up to now, hollow spherical structures have easily been achieved through conventional hard-template,[2] soft-template,[3] sacrificial-template,[4] and template-free methods.[5] Compared to spherical counterparts, however, the synthesis of hollow crystals with nonspherical shapes remains a significant challenge to material scientists because of the difficulties in employing template technologies.[6] There are only limited successes in the synthesis of nonspherical hollow crystals through the template-free route as well. For example, hollow spindle-shaped hematite crystals could be fabricated by the selective dissolution of the interiors under hydrothermal conditions with the exterior protected by adsorbed phosphate anions.[7]

$BiVO_4$ has stimulated scientists' tremendous interest because of its unique properties, such as ferroelasticity,[8] ionic conductivity,[9] gas sensing,[10] and coloristic properties.[11] Moreover, it has also been considered as one of the excellent visible-light-responsive photocatalysts and widely applied in

*To whom correspondence should be addressed. E-mail: dkma@wzu.edu.cn (D.-K.M.), smhuang@wzu.edu.cn (S.-M.H.). Fax: +86 577 88373064. Tel: +86 577 88373031.

(1) (a) Caruso, F.; Caruso, R. A.; Möhwald, H. *Science* **1998**, *282*, 1111. (b) Mathiowitz, E.; Jacob, J. S.; Jong, Y. S.; Carino, G. P.; Chickering, D. E.; Chaturvedi, P.; Santos, C. A.; Vijayaraghavan, K.; Montgomery, S. *Nature* **1997**, *386*, 410. (c) Lou, X. W.; Wang, Y.; Yuan, C.; Lee, J. Y.; Archer, L. A. *Adv. Mater.* **2006**, *18*, 2325. (d) Li, H. X.; Bian, Z. F.; Zhu, J.; Zhang, D. Q.; Li, G. S.; Huo, Y. N.; Li, H.; Lu, Y. F. *J. Am. Chem. Soc.* **2007**, *129*, 8406. (e) Kim, S. W.; Kim, M.; Lee, W. Y.; Hyeon, T. *J. Am. Chem. Soc.* **2002**, *124*, 7642. (f) Zhang, H. G.; Zhu, Q. S.; Zhang, Y.; Wang, Y.; Zhao, L.; Yu, B. *Adv. Funct. Mater.* **2007**, *17*, 2766. (g) Chen, J.; Saeki, F. B.; Wiley, J.; Cang, H.; Cobb, M. J.; Li, Z. Y.; Au, L.; Zhang, H.; Kimmey, M. B.; Li, X. D.; Xia, Y. N. *Nano Lett.* **2005**, *5*, 473.
(2) Wolosiuk, A.; Armagan, O.; Braun, P. V. *J. Am. Chem. Soc.* **2005**, *127*, 16356.
(3) Zhang, D. B.; Qi, L. M.; Ma, J. M.; Cheng, H. M. *Adv. Mater.* **2002**, *14*, 1499.
(4) Jeong, U. Y.; Xia, Y. N. *Angew. Chem., Int. Ed.* **2005**, *44*, 3099.
(5) Li, J.; Zeng, H. C. *Angew. Chem., Int. Ed.* **2005**, *44*, 4342.
(6) Lou, X. W.; Archer, L. A.; Yang, Z. C. *Adv. Mater.* **2008**, *20*, 1.
(7) Jia, C. J.; Sun, L. D.; Yan, Z. G.; You, L. P.; Luo, F.; Han, X. D.; Pang, Y. C.; Zhang, Z.; Yan, C. H. *Angew. Chem., Int. Ed.* **2005**, *44*, 4328.
(8) David, W. I. F.; Wood, I. G. *J. Phys. C: Solid State Phys.* **1983**, *16*, 5149.
(9) Hirota, K.; Komatsu, G.; Yamashita, M.; Takemura, H.; Yamaguchi, O. *Mater. Res. Bull.* **1992**, *27*, 823.
(10) Zhao, Y.; Xie, Y.; Zhu, X.; Yan, S.; Wang, S. X. *Chem.—Eur. J.* **2008**, *14*, 1601.
(11) Zhang, L.; Chen, D. R.; Jiao, X. L. *J. Phys. Chem. B* **2006**, *110*, 2668.

 Published on Web 12/20/2010

the photocatalytic evolution of O_2 and degradation of organic pollutants.[12] The photocatalytic properties of $BiVO_4$ are strongly dependent on its morphologies and microstructures.[13] Therefore, many efforts have been made to synthesize $BiVO_4$ with various morphologies, such as three-dimensional mesocrystals,[14] hyperbranched structures,[10] hierarchical microspheres,[15] nanotubes,[16] and nanoplates.[17] In addition, the photocatalytic properties of $BiVO_4$ are closely related to the phase structures.[18] There are three crystalline phases reported for synthetic $BiVO_4$, namely, a tetragonal zircon structure, a monoclinic scheelite structure, and a tetragonal scheelite structure. Among these phase structures, the monoclinic scheelite structure of $BiVO_4$ possesses the best photocatalytic performance under visible-light irradiation. However, its photocatalytic activity is not ideal yet because of the difficult migration of photogenerated electrons and holes and thus needs to be further improved for practical application.

Composite semiconductors can reduce the recombination probability of photogenerated electrons and holes and thus have been widely employed to improve the photocatalytic activity of materials.[19] Among various composite photocatalysts, the fabrication of a p−n heterojunction has been demonstrated as a very efficient means of separating electron−hole pairs because of the internal electric field with the direction from an n-type semiconductor to a p-type semiconductor.[20] $BiVO_4$ is intrinsic n-type semiconductor and Bi_2O_3 is intrinsic p-type semiconductor with good photocatalytic activity. Theoretically, a p−n heterojunction will form when n-type $BiVO_4$ and p-type Bi_2O_3 semiconductors combine together. However, up to now, there are few reports on p−n Bi_2O_3/$BiVO_4$ composite photocatalysts. Especially, a core−shell heterojunction of the composite photocatalysts, to the best of our knowledge, has never been reported. Recently, Li et al. reported that Bi_2O_3/$BiVO_4$ submicrometer spheres prepared by the direct mixture of Bi_2O_3 and $BiVO_4$ could show much higher photocatalytic activities than pure Bi_2O_3 and $BiVO_4$.[21] However, it is difficult to form an efficient and sound heterojunction with the physical mixture, which is crucial to improving the photocatalytic efficiency of the materials.[20]

In this study, we represent a mixed solvothermal route to synthesize hollow olive-shaped $BiVO_4$ with a monoclinic scheelite structure through a sodium bis(2-ethylhexyl)sulfosuccinate (AOT)-induced aggregate and Ostwald ripening process, free of templates, seeds, and catalysts. Subsequently, n−p core−shell $BiVO_4$@Bi_2O_3 was fabricated by a thermal aqueous solution etching process under hydrothermal conditions, employing olive-shaped $BiVO_4$ as a precursor. Furthermore, the photocatalytic activities of hollow olive-shaped $BiVO_4$ and n−p core−shell $BiVO_4$@Bi_2O_3 microspheres were contrastively studied.

Experimental Section

I. Synthesis of Hollow Olive-Shaped $BiVO_4$. A total of 1 mmol of $Bi(NO_3)_3 \cdot 5H_2O$ was added into 40 mL of mixed solvents (ultrapure water and ethylene glycol with a volume ratio of 1:1) under agitation. Then 1 mmol of $NaVO_3 \cdot 2H_2O$ and 3 mmol of AOT were introduced into the solution in sequence. After more agitation for 5 min, the solution was poured into a stainless steel autoclave with a Teflon liner of 50 mL capability and heated at 160 °C for 18 h. After the autoclave was cooled to room temperature, the products were separated centrifugally and washed with ultrapure water and absolute ethanol three times. Then the products were dried under vacuum at 60 °C for 4 h.

II. Synthesis of Core−Shell $BiVO_4$@Bi_2O_3. A total of 0.5 mmol of the as-obtained olive-shaped $BiVO_4$ powders was dispersed in 40 mL of ultrapure water under vigorous stirring. Then 5 mmol of NaOH was added into the solution. After stirring for a while, the solution was poured into a stainless steel autoclave with a Teflon liner of 50 mL capacity, sealed, and heated at 180 °C for 12 h. The post-treatment process of the sample is the same as that of olive-shaped $BiVO_4$.

III. Characterization. Powder X-ray diffraction (XRD) was carried out with a Bruker D8 Advance X-ray diffractometer using Cu Kα radiation (λ = 0.154 18 nm) at a scanning rate of 8°/min in the 2θ range of 10−70°. Field-emission scanning electron microscopy (FE-SEM) images were taken on a Nova NanoSEM 200 scanning electron microscope. Transmission electron microscopy (TEM) observations, energy-dispersive X-ray (EDX) spectroscopy, and high-resolution TEM (HRTEM) images were performed with a JEOL JEM 2010 high-resolution transmission electron microscope, using an accelerating voltage of 200 kV. The optical diffuse-reflectance spectra were recorded on a UV2501PC (Shimadzu) using $BaSO_4$ as a reference. The Brunauer−Emmett−Teller (BET) surface area was measured with a ASAP2020 specific surface area and porosity analyzer. Photoelectrochemistry measurements were carried out in a three-electrode cell with a flat quartz window using an electrochemical system (CH1660C). The $BiVO_4$ films prepared by olive-shaped $BiVO_4$ and the Bi_2O_3 films prepared by Bi_2O_3 nanoplates (obtained by hydrothermal complete etching of $BiVO_4$ with 20 mmol of NaOH at 220 °C) were used as working electrodes. A platinum wire and saturated calomel electrode were used as counter and reference electrodes, respectively. A 0.1 M Na_2SO_4 aqueous solution was used as an electrolyte. A 500 W Xe light with a 400 nm cutoff filter was used as the visible-light source.

IV. Photocatalytic Properties Study. The photocatalytic activities of olive-shaped $BiVO_4$ and core−shell $BiVO_4$@Bi_2O_3 were evaluated by degradation of rhodamine B (RhB) under visible-light irradiation from 500 W Xe light (CHF-XM500, purchased from Beijing Lituo Science and Technology Co. Ltd.) equipped with a 400 nm cutoff filter. In every experiment, 100 mg of photocatalysts were added to 100 mL of a RhB solution (10^{-5} mol/L). Before illumination, the solution was magnetically stirred in the dark for 2 h to ensure the establishment of an adsorption−desorption equilibrium between the photocatalysts and RhB. After that, the solution was exposed to visible-light irradiation under magnetic stirring. At given time intervals, 3 mL aliquots were sampled and centrifuged to remove the photocatalyst particles. Then, the filtrates were analyzed by recording variations of the absorption band maximum (553 nm) in the UV−vis spectra of RhB by using a Shimadzu UV2501PC spectrophotometer.

(12) (a) Kudo, A.; Omori, K.; Kato, H. *J. Am. Chem. Soc.* **1999**, *121*, 11459. (b) Li, G. S.; Zhang, D. Q.; Yu, J. C. *Chem. Mater.* **2008**, *20*, 3983.
(13) (a) Tokunaga, S.; Kato, H.; Kudo, A. *Chem. Mater.* **2001**, *13*, 4624. (b) Zhou, L.; Wang, W. Z.; Liu, S. W.; Zhang, L. S.; Xu, H. L.; Zhu, W. *J. Mol. Catal. A* **2006**, *252*, 120.
(14) Zhou, L.; Wang, W. Z.; Xu, H. L. *Cryst. Growth Des.* **2008**, *8*, 728.
(15) Ma, D. K.; Wang, S.; Cai, P.; Jiang, J. L.; Yang, D. P.; Huang, S. M. *Chem. Lett.* **2009**, *38*, 962.
(16) Ren, L.; Jin, L.; Wang, J. B.; Yang, F.; Qiu, M. Q.; Yu, Y. *Nanotechnology* **2009**, *20*, 115603.
(17) Xi, G. C.; Ye, J. H. *Chem. Commun.* **2010**, *46*, 1893.
(18) Zhang, X.; Ai, Z. H.; Jia, F. L.; Zhang, L. Z.; Fan, X. X.; Zou, Z. G. *Mater. Chem. Phys.* **2007**, *103*, 162.
(19) Ni, M.; Leung, M. K. H.; Leung, D. Y. C.; Sumathy, K. *Renewable Sustainable Energy Rev.* **2007**, *11*, 401.
(20) (a) Kim, H. G..; Pramod, H. B.; Lee, J. S. *Angew. Chem., Int. Ed.* **2005**, *44*, 4585. (b) Long, M. C.; Cai, W. M.; Cai, J.; Zhou, B. X.; Chai, X. Y.; Wu, Y. H. *J. Phys. Chem. B* **2006**, *110*, 20211. (c) Ahn, K. S.; Yan, Y. F.; Kang, M. S.; Kim, J. Y.; Shet, S.; Wang, H. L.; Turner, J.; Al-Jassim, M. *Appl. Phys. Lett.* **2009**, *95*, 022116.
(21) Li, L. Z.; Yan, B. *J. Alloys Compd.* **2009**, *476*, 624.

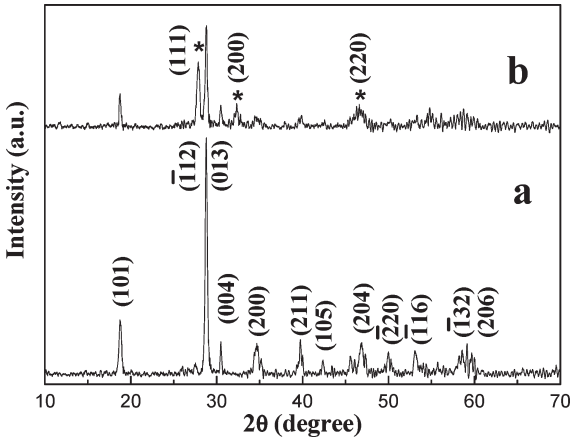

Figure 1. Powder XRD patterns of the products synthesized by a mixed solvothermal route (a) and a thermal solution of NaOH etching process (b).

Results and Discussion

The crystallinity and phase purity of the as-obtained products were examined by XRD measurements. As can be seen from Figure 1a, all of the reflections of the products obtained by an AOT-assisted mixed solvothermal route can be readily indexed to a pure monoclinic scheelite structure of $BiVO_4$ [space group *I*2/*b*], which is in good agreement with the reported data (JCPDS No. 75-2480). After being etched by a thermal solution of NaOH under hydrothermal conditions, monoclinic $BiVO_4$ was partially changed into cubic Bi_2O_3 (asterisks denote Bi_2O_3; JCPDS No. 27-0052), as shown in Figure 1b.

Panels a and b of Figure 2 represent panoramic and high-magnification FE-SEM images of the as-obtained $BiVO_4$ products, respectively. From Figure 2a, it can be seen that the products consist of large numbers of uniform olive-shaped particles. The diameters of the individual olive along long and short axis directions are 1−1.5 and 0.6−0.9 μm, respectively. The magnified FE-SEM image shows that the products have hollow interiors (Figure 2b), judged from broken particles. TEM images were further used to confirm this point. As shown in Figure 2c, the obvious contrast of brightness in olive-shaped microspheres assuredly means the formation of cavities in the light region. Careful FE-SEM observations of a total of 500 olive-shaped microspheres indicate that 54 microspheres (ca. 10%) are open. After the olive-shaped $BiVO_4$ microspheres were etched by a thermal solution of NaOH, core−shell microspheres were formed, as shown in the TEM images in Figure 2d. The magnified TEM image (inset in the upper-right corner) more clearly shows distinct bright/dark contrast between the shell and core. HRTEM was further used to characterize the as-synthesized core−shell structures. Figure 2e is a HRTEM image taken from the edge of an individual microsphere. The spacings of the adjacent lattice planes are ca. 3.20 and 2.79 Å, which are consistent with the interplanar spacings of (111) and (200) planes of cubic Bi_2O_3, respectively. The EDX spectra recorded on the individual microspheres were carried out as well (see the Supporting Information, Figure S1). The ratio of Bi to V is ca. 65.58:34.42 on the basis of the results of calculation. This further shows that the microsphere consists of Bi_2O_3 and $BiVO_4$. According to the above-mentioned results, it is known that the core and shell correspond to $BiVO_4$ and Bi_2O_3, respectively.

In the present system, AOT plays a key role in the formation process of olive-shaped $BiVO_4$. Keeping other conditions

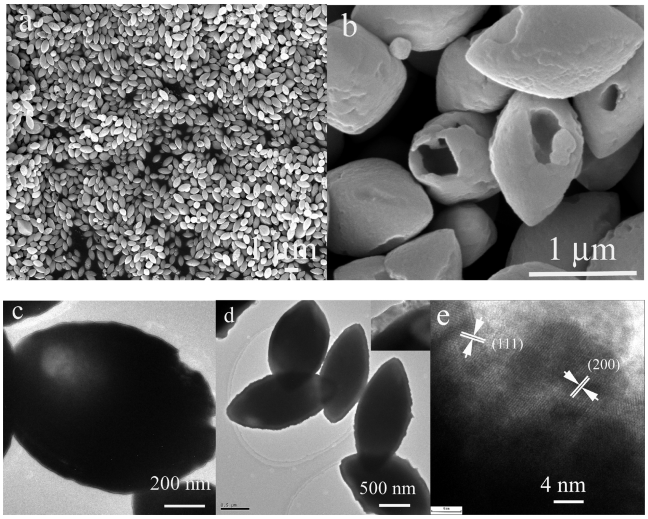

Figure 2. Panoramic (a) and high-magnification (b) FE-SEM images and TEM image (c) of the as-obtained $BiVO_4$ products. (d) Panoramic TEM image of the products synthesized by a thermal solution of NaOH etching process under hydrothermal conditions. The inset is a magnified TEM image performed on the rim of an individual microsphere. (e) HRTEM image taken from the edge of a single core−shell microsphere.

unchanged, in the absence of AOT, the resultant products consist of predominant bone-shaped microcrystals (Figure S2a in the Supporting Information). It was also found that the volume ratios of water to ethylene glycol had an obvious influence on the morphologies of the final products. When the volume ratio of ethylene glycol to water was increased from 1:3, to 1:1, to 3:1, the resultant products took on star-shaped (Figure S2b in the Supporting Information), uniform olive-shaped (Figure S2c in the Supporting Information), and irregular olive-shaped morphologies (Figure S2d in the Supporting Information) in sequence. Ethylene glycol has been successfully used to control the morphologies of various metal oxides by a coordination action with transition-metal ions.[22] In the experimental process, we observed that the aqueous solution became white turbid when $Bi(NO_3)_3 \cdot 5H_2O$ was added in water. This was due to the formation of slightly soluble $BiONO_3$ as a result of $Bi(NO_3)_3$ hydrolysis.[23] With the introduction of ethylene glycol into the solution, the turbid solution gradually became clear under agitation. This phenomenon indicates that $BiONO_3$ was dissolved and a coordination action between Bi^{3+} ions with ethylene glycol molecules took place. On the other hand, the solubilities of the reactants and products in water and ethylene glycol were different. Therefore, the nucleation and growth rate of the crystals could be adjusted by modulating the volume ratios of mixed solvents. As a result, as in some previous reports,[24] different morphologies of $BiVO_4$ could be produced under mixed solvothermal conditions.

In order to understand the morphological evolution process of hollow olive-shaped $BiVO_4$, XRD analyses and SEM

(22) (a) Jiang, X. C.; Wang, Y. L.; Herricks, T.; Xia, Y. N. *J. Mater. Chem.* **2004**, *14*, 695. (b) Scott, R. W. J.; Coombs, N.; Ozin, G. A. *J. Mater. Chem.* **2003**, *13*, 969.

(23) Ma, D. K.; Huang, S. M.; Chen, W. X.; Hu, S. W.; Shi, F. F.; Fan, K. L. *J. Phys. Chem. C* **2009**, *113*, 4369.

(24) (a) Liu, Z. P.; Peng, S.; Xie, Q.; Hu, Z. K.; Yang, Y.; Zhang, S. Y.; Qian, Y. T. *Adv. Mater.* **2003**, *15*, 936. (b) Yao, W. T.; Yu, S. H.; Pan, L.; Li, J.; Wu, Q. S.; Zhang, L.; Jiang, J. *Small* **2005**, *1*, 320. (c) Yao, W. T.; Yu, S. H.; Huang, X. Y.; Jiang, J.; Zhao, L. Q.; Pan, L.; Li, J. *Adv. Mater.* **2005**, *17*, 2799.

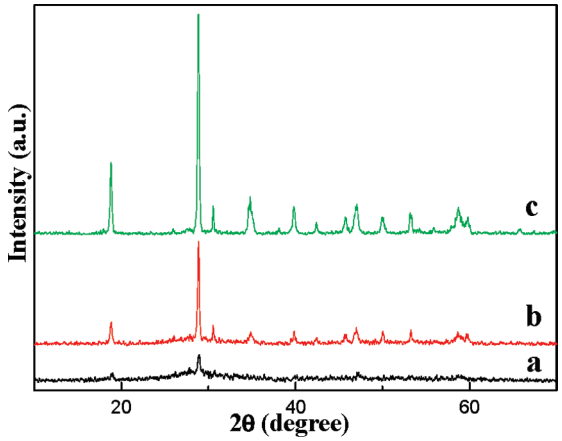

Figure 3. Powder XRD patterns of the products synthesized at different reaction stages: (a) 30 min; (b) 1 h; (c) 3 h.

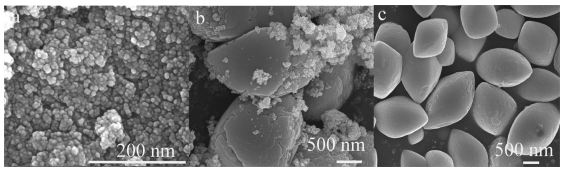

Figure 4. FE-SEM images of the products synthesized at different reaction stages: (a) 30 min; (b) 1 h; (c) 3 h.

observations at different reaction stages were carried out. Figures 3 and 4 represent XRD patterns and corresponding FE-SEM images of the samples synthesized for 30 min and 1 and 3 h, respectively. As can be seen from these patterns and FE-SEM images, the products are poor-crystalline nanoparticles within the initial 30 min. With the reaction time extended to 1 h, these amorphous nanoparticles have begun to aggregate together and form some olive-shaped spheres. As the reaction time was prolonged to 3 h, the products have grown into well-defined and crystalline olive-shaped microspheres. On the basis of the above results, the possible formation process of olive-shaped $BiVO_4$ spheres was proposed as follows. At the initial stage of the reaction, Bi^{3+} with VO_4^{3-} ions precipitated quickly under the driving force of low-solubility products of $BiVO_4$. Subsequently, the newborn nanoparticles aggregated into loose olive-shaped microspheres under the inducement action of AOT molecules absorbed on nanoparticles' surfaces through intermolecular interaction. Finally, inside-out Ostwald ripening among these amorphous nanoparticles took place because the surfaces of the nanoparticles were in contact with the surrounding solution. As a result, the interior nanoparticles have a tendency to dissolve, which provides the driving force for spontaneous inside-out Ostwald ripening.[1c] This dissolution process could initiate at regions either near the surface or around the center of the olive-shaped microspheres, presumably depending on the packing of primary nanoparticles and ripening characteristics, to produce olive-shaped hollow spheres. A simple schematic illustration for formation of the process is given in Scheme 1.

The energy band structure feature of a semiconductor is considered the key factor in determining its photocatalytic activity. Figure 5a shows the UV−vis diffuse-reflectance spectra of the as-synthesized olive-shaped $BiVO_4$ and core−shell $BiVO_4@Bi_2O_3$ microspheres, respectively. Both of the samples show strong absorption in the UV- and visible-light

Scheme 1. Possible Formation Process of Hollow Olive-Shaped $BiVO_4$ Microspheres

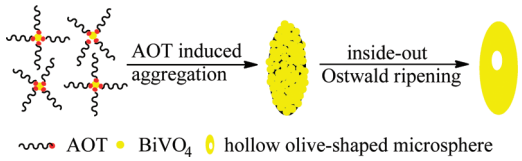

regions. The steep absorption edge of the two spectra indicates that the visible-light adsorption is not due to the transition from the impurity level but to the band-gap transition. Their band gaps could be determined with the formula $\alpha h\nu = A(h\nu - E_g)^{n/2}$, where α, h, ν, A, E_g, and n are the absorption coefficient, Planck's constant, the incident light frequency, a constant, the band-gap energy, and an integer, respectively. Among them, n depends on the characteristics of the optical transition in a semiconductor, i.e., direct transition ($n = 1$) or indirect transition ($n = 4$). For $BiVO_4$ and Bi_2O_3, both of them pertain to direct transition and the values of n are 1.[13b,25] The band-gap energy (E_g value) of $BiVO_4$ can be thus estimated from a plot of $(\alpha h\nu)^2$ versus the photon energy ($h\nu$). The intercept of the tangent to the x axis will give a good approximation of the band-gap energy for the olive-shaped $BiVO_4$ and core−shell $BiVO_4@Bi_2O_3$, as shown in Figure 5b. The estimated band-gap energies of the as-obtained $BiVO_4$ and core−shell $BiVO_4@Bi_2O_3$ were about 2.43 and 2.52 eV from the absorption onsets, respectively. The band-gap energy of olive-shaped $BiVO_4$ microspheres is close to that of $BiVO_4$ microtubes reported previously (2.36 eV).[26] According to previous reports, Bi_2O_3 nanoparticles with sizes of 40−100 nm have a band-gap energy of ca. 2.85 eV.[27] The Bi_2O_3 shell has a thickness of ca. 90 nm. Therefore, its band-gap energy can be approximately estimated to be ca. 2.85 eV as well. As a result, the core−shell $BiVO_4@Bi_2O_3$ has a larger band-gap energy than single-phase olive-shaped $BiVO_4$ and a smaller one than Bi_2O_3.

In order to evaluate the photocatalytic activities of the as-synthesized olive-shaped $BiVO_4$ and core−shell $BiVO_4@Bi_2O_3$, the degradation ability of RhB dye in water under visible-light irradiation was studied. Parts a and b of Figure 6 show the temporal evolution of the UV−vis spectra during photodegradation of RhB on olive-shaped $BiVO_4$ and core−shell $BiVO_4@Bi_2O_3$ microspheres under visible-light irradiation ($\lambda > 400$ nm). As can be seen from the above two spectra, absorption of both RhB/olive-shaped $BiVO_4$ and RhB/core−shell $BiVO_4$ suspensions gradually decreased during photodegradation. In addition, the major absorption peak corresponding to RhB was shifted from 553 to 496 nm step by step, indicating the removal of ethyl groups one by one, which was in agreement with the literature.[28] The corresponding plots for the concentration changes of RhB determined from its characteristic absorption peak (at 553 nm) are shown in Figure 6c. It is obvious that core−shell $BiVO_4@Bi_2O_3$ shows higher photocatalytic activities than olive-shaped $BiVO_4$ under identical experimental conditions.

(25) Zhou, L.; Wang, W. Z.; Xu, H. L.; Sun, S. M.; Shang, M. *Chem.—Eur. J.* **2009**, *15*, 1776.
(26) Zhou, L.; Wang, W. Z.; Zhang, L. S.; Xu, H. L.; Zhu, W. *J. Phys. Chem. C* **2007**, *111*, 13659.
(27) Zhang, L. S.; Wang, W. Z.; Yang, J.; Chen, Z. G.; Zhang, W. Q.; Zhou, L.; Liu, S. W. *Appl. Catal., A* **2006**, *308*, 105.
(28) (a) Zhao, W.; Chen, C.; Li, X.; Zhao, J. C. *J. Phys. Chem. B* **2002**, *106*, 5022. (b) Zhang, C.; Zhu, Y. F. *Chem. Mater.* **2005**, *17*, 3537.

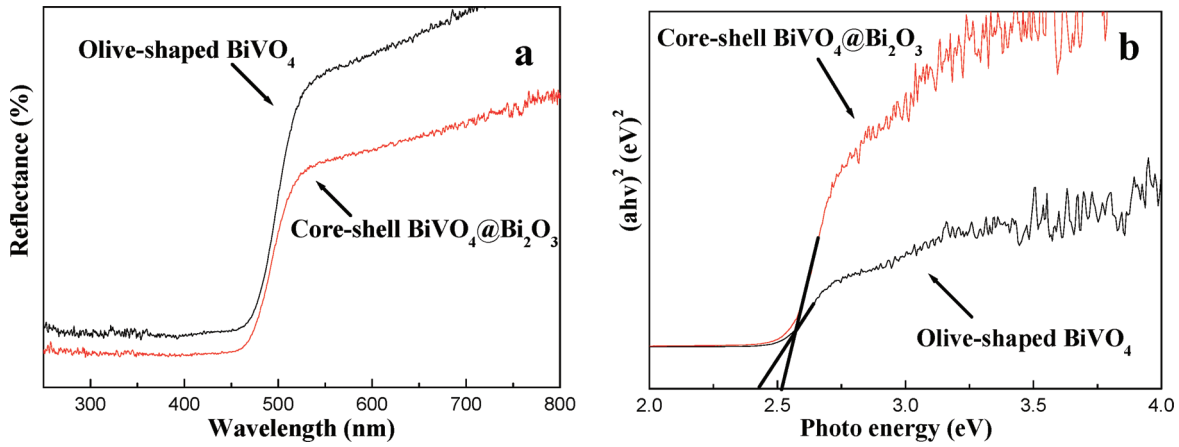

Figure 5. UV−vis diffuse-reflectance spectra (a) and plots of $(\alpha h\nu)^2$ versus the photon energy ($h\nu$) (b) of the as-synthesized olive-shaped $BiVO_4$ and core−shell $BiVO_4@Bi_2O_3$ microspheres.

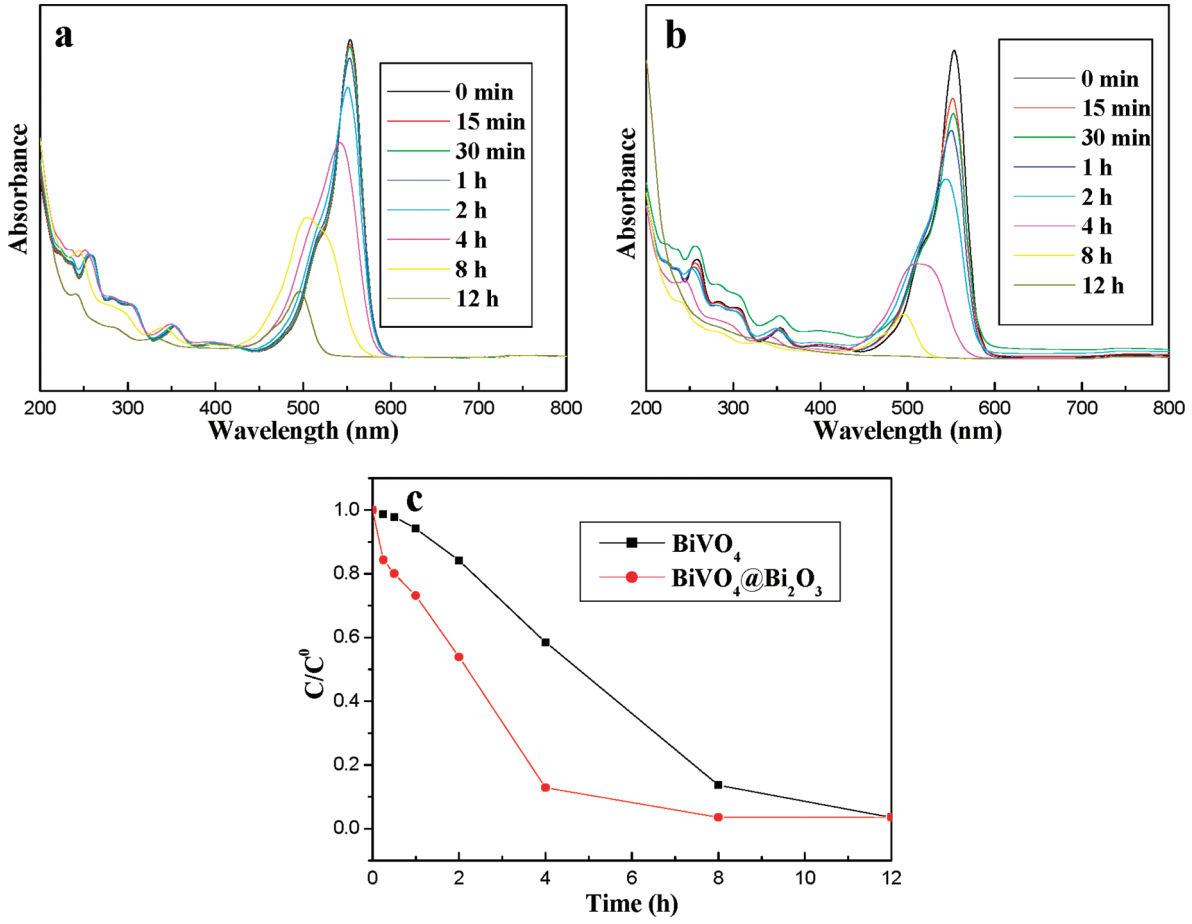

Figure 6. Changes of UV−vis spectra of olive-shaped $BiVO_4$ (a) and core−shell $BiVO_4@Bi_2O_3$ microspheres (b) suspended in a RhB solution as a function of the irradiation time and RhB concentration changes over olive-shaped $BiVO_4$ and core−shell $BiVO_4@Bi_2O_3$ microspheres (c), respectively.

Why does core−shell $BiVO_4@Bi_2O_3$ exhibit superior photocatalytic activity over olive-shaped $BiVO_4$? It is well-known that the activities of photocatalysts mostly depend on the specific surface area, light energy utilization ratio, and quantum efficiency. The larger the surface area of the materials, the higher the photocatalytic activity they show. On the basis of the N_2 adsorption−desorption isotherms, the calculated BET surface areas of olive-shaped $BiVO_4$ and core−shell $BiVO_4@Bi_2O_3$ are 1.4451 and 1.4810 m^2/g, respectively. They show almost the same surface area. The responsive range of visible light for $BiVO_4@Bi_2O_3$ is narrower than that of olive-shaped $BiVO_4$. The control experiment also reveals that Bi_2O_3 hierarchical architectures composed of nanosheets with much higher surface area (33.1 m^2/g) exhibit an photocatalytic performance inferior to that of core−shell $BiVO_4@Bi_2O_3$ under the same measurement conditions (see the Supporting Information, experimental part and Figure S3−S5). Therefore, the enhanced photocatalytic activity of $BiVO_4@Bi_2O_3$ is most possibly related to the core−shell heterojunction between $BiVO_4$ and Bi_2O_3. According to photoelectrochemical

Scheme 2. Diagram for Band Levels of Core−Shell $BiVO_4$@Bi_2O_3 Composites and the Possible Charge-Separation Process

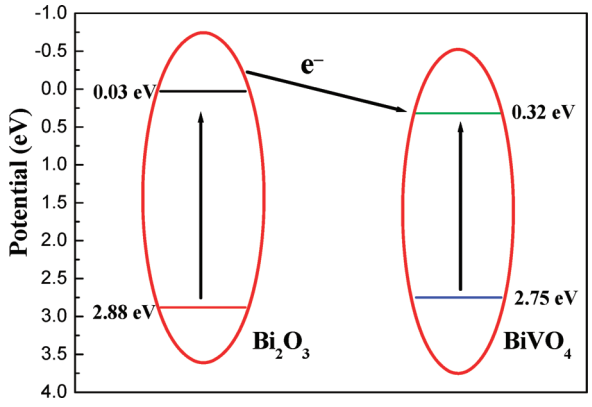

measurements (see Figures S6 and S7 in the Supporting Information), olive-shaped $BiVO_4$ and Bi_2O_3 nanoplates respectively show anodic and cathodic photocurrents when the light is on, indicating that $BiVO_4$ is an n-type semiconductor and Bi_2O_3 is a p-type semiconductor. When they were combined, a p−n-type heterojunction would be produced. In recent years, this kind of p−n composite photocatalyst has been used to reduce the recombination probability of photogenerated electrons and holes via the internal electric field and thus lead to a high quantum yield.[20] However, whether it is valid to separate photogenerated charge carriers strongly depends on the band-edge positions of the two semiconductors. The conduction band edge of a semiconductor at the point of zero charge can be calculated by the empirical equation $E_{VB} = X - E^e + 0.5E_g$,[29] where E_{VB} is the valence band-edge potential, X is the electronegativity of the semiconductor, expressed as the geometric mean of the absolute electronegativity of the constituent atoms, E^e is the energy of free electrons on the hydrogen scale (about 4.5 eV), E_g is the band-gap energy of the semiconductor, and E_{CB} can be determined by $E_{CB} = E_{VB} - E_g$. The X values for $BiVO_4$ and Bi_2O_3 are ca. 6.04 and 5.95 eV. The band-gap energies of $BiVO_4$ and Bi_2O_3 adopt 2.43 and 2.85 eV, respectively. Given the equation above, the top of the valence band and the bottom of the conduction band of $BiVO_4$ and Bi_2O_3 are calculated to be 0.32 and 2.75 eV and 0.03 and 2.88 eV, respectively. According to the above results, Scheme 2 was proposed to illustrate a possible charge-separation process. As shown in Scheme 2, both $BiVO_4$ and Bi_2O_3 could be easily excited by visible light ($\lambda > 400$ nm) and induce the generation of electron and hole pairs. However, the conduction band-edge potential of Bi_2O_3 (0.03 eV) is more active than that of $BiVO_4$ (0.32 eV). Therefore, photoinduced electrons on the surfaces of Bi_2O_3 would easily transfer to $BiVO_4$ under the inducement action of the internal p−n electric field, leaving holes on the Bi_2O_3 valence band. In such a way, the photoinduced electrons and holes could be effectively separated. Therefore, according to the above results, the higher photocatalytic activity of core−shell $BiVO_4$@Bi_2O_3 than of single-phase $BiVO_4$ and Bi_2O_3 could be mostly ascribed to an enhanced quantum efficiency, i.e., efficient separation of photogenerated carriers via a p−n heterojunction. The detailed reasons need to be clarified, and further study is underway.

(29) (a) Bulter, M. A.; Ginley, D. S. *J. Electrochem. Soc.* **1978**, *125*, 228. (b) Cheng, H. F.; Huang, B. B.; Dai, Y.; Qin, X. Y.; Zhang, X. Y. *Langmuir* **2010**, *26*, 6618.

Conclusions

In summary, hollow olive-shaped $BiVO_4$ and core−shell $BiVO_4$@Bi_2O_3 microspheres have been successfully synthesized by an AOT-assisted mixed solvothermal route and thermal solution etching method under hydrothermal conditions, respectively. In order to obtain well-defined olive-shaped $BiVO_4$ microspheres, the use of AOT and the selection of appropriate solvent ratios are indispensable. On the basis of analysis of the temporal evolution process, the formation of olive-shaped $BiVO_4$ probably went through AOT-molecule-induced aggregation and an inside-out Ostwald ripening process. Both olive-shaped $BiVO_4$ and core−shell $BiVO_4$@Bi_2O_3 microspheres exhibited visible-light-responsive photocatalytic activities, while the latter showed much higher activity under the same experimental conditions. According to the calculated band-edge positions of the two semiconductors, the enhanced activity of core−shell $BiVO_4$@Bi_2O_3 microspheres can be mostly attributed to the p−n heterojunction structure and thus the reduced recombination probability of photogenerated hole−electron carriers. The present core−shell $BiVO_4$@Bi_2O_3 microspheres are promising applications in the field of environmental remediation for good visible-light-responsive photocatalytic activity and easy separation.

Acknowledgment. The authors appreciate partial financial support from NSFZJ (Grants Y4090118 and R4090137), the ZJED Innovative Team, and NSFC (Grants 51002107 and 50772076).

Supporting Information Available: EDX spectroscopy recorded on an individual microsphere, FE-SEM images of the products under different synthetic conditions, experimental part for the synthesis and photocatalytic activity testing of Bi_2O_3 with hierarchical architectures, FE-SEM image of the as-obtained Bi_2O_3, UV−vis spectra of Bi_2O_3 hierarchical architectures suspended in a RhB solution as a function of the irradiation time, plots for RhB concentration changes over olive-shaped $BiVO_4$, core−shell $BiVO_4$@Bi_2O_3 microspheres, and Bi_2O_3 hierarchical architectures, and measured $I-V$ curves for pure $BiVO_4$ and Bi_2O_3, respectively. This material is available free of charge via the Internet at http://pubs.acs.org.